PAPER

Graphene film doped with silver nanoparticles: self-assembly formation, structural characterizations, antibacterial ability, and biocompatibility

Panpan Zhang,[a] Haixia Wang,[a] Xiaoyuan Zhang,[a,b] Wei Xu,[a] Yang Li,[a] Qing Li,[c] Gang Wei*[c] and Zhiqiang Su*[a]

Graphene and silver nanoparticles (AgNPs) are important building blocks for the synthesis of functional nanomaterials for bio-related applications. Here, we report a facile strategy to decorate AgNPs onto reduced graphene oxide (RGO) by the simultaneous reduction of silver ions and graphene oxide nanosheets within one system, and further to fabricate a dimension-adjustable RGO/AgNP multi-layered film by a thermal-driven self-assembly process. The structures of the fabricated RGO/AgNP hybrid films were identified by UV-visible spectroscopy, X-ray diffraction, X-ray photoelectron spectroscopy, Raman spectroscopy, and transmission electron microscopy. The thickness of the fabricated RGO/AgNP film was further measured by scanning electron microscopy. The hydrophilicity of the RGO/AgNP films was tested by contact angle measurement. Antibacterial and cell culture experiments based on the fabricated RGO/AgNP films indicate that this kind of hybrid film exhibits excellent antibacterial activity and high biocompatibility. A potential antibacterial mechanism of the fabricated RGO/AgNP hybrid film was proposed.

1. Introduction

With increasing concern about medical and surgical risks, microbial infections have been hot research fields following the urgent demands of efficient, innoxious, and secure antibacterial materials.[1–3] Antibacterial materials can be mainly divided into two types: organic and inorganic. Inorganic antibacterial materials have attracted more interest compared to organic ones due to their better heat-durability, longer validity, and higher stability.[4–6] With the development of nanotechnology, many kinds of nanomaterials have been synthesized for antibacterial applications.[7–11] Antibacterial nanomaterials possess more excellent and comprehensive performances ascribing their novel and enhanced properties as being related to the nanoscale effect. Until now, inorganic nanomaterials such as titanium dioxide (TiO_2),[7] zinc oxide (ZnO),[6,8] silver[9,10] and copper[11] nanoparticles (AgNPs and CuNPs) have been found to have very good antibacterial activities. For instance, Krishnaraj et al. used Acalypha indica extracted from leaves to

biomimetically synthesize AgNPs with a size of 20–30 nm, and further demonstrated that the synthesized AgNPs have effective inhibitory activity against bacterial-like water borne pathogens viz., Escherichia coli and Vibrio cholerae.[10]

Throughout the past few decades, Ag-based nanomaterials have occupied an important position as remarkable antibacterial agents. In addition, a great number of Ag-containing composited nanomaterials for antibacterial application have been reported.[12,13] For example, Pinto et al. prepared cellulose/Ag composites and discovered their excellent antibacterial activity for Bacillus subtilis, Staphylococcus aureus and Klebsiella pneumoniae.[12] Recently, Fei and co-workers used Bombyx mori silk fibroin as a template to in situ produce AgNPs under light, and the silk fibroin/AgNP composite destroyed the methicillin-resistant Staphylococcus aureus.[13] Although many materials have been used as substrates and templates for binding with AgNPs to synthesize effective antibacterial nanomaterials, the hybridization of AgNPs with graphene and its derivatives still have potential significances as a novel antibacterial nanomaterial.

Graphene and its derivatives have been widely used for the varied research fields such as optoelectronics, energy resources, nanotechnology, and biotechnology ascribing to their excellent macroscopic and microcosmic properties.[14,15] There is increasing interest for the preparation and application of novel graphene-based nanomaterials, especially hybrid

[a]State Key Laboratory of Chemical Resource Engineering, Beijing University of Chemical Technology, 100029 Beijing, China. E-mail: suzq@mail.buct.edu.cn
[b]Chair of Materials Science, Otto Schott Institute of Materials Research, Friedrich-Schiller-University Jena, D-07743 Jena, Germany
[c]Hybrid Materials Interfaces Group, Faculty of Production Engineering, University of Bremen, D-28359 Bremen, Germany. E-mail: wei@uni-bremen.de

graphene film decorated with other building nanoblocks.[16,17] Indeed, compared to bulk composites, hybrid films have multiple advantages of lighter weight, smaller volume, larger specific surface area, and easier preparation. Recently, the potential conductive applications of graphene-based hybrid films, such as with a conductor,[18] electrode,[19] sensor,[20,21] and battery,[22] have attracted much more interest while the antibacterial and cellular bioapplications gained comparatively less attention.

Although the questions whether and how graphene and its derivatives present antibacterial activity are still not clear, graphene-based hybrid film may achieve significant discoveries in biological applications.[23,24] With AgNPs attaching onto the lamellar structure of reduced graphene oxide (RGO) as a substrate, the RGO/AgNP hybrid films demonstrated enhanced antibacterial activities.[25–27] For example, Hu *et al.* found superior antibacterial effects with graphene-based paper, which was responsible for the bacteria-killing effect of a fabricated graphene-based paper.[25] With incorporation of AgNPs onto GO sheets, Ma and co-workers found that the modified GO nanosheets provided enhanced antibacterial activity by the synergistic effects of AgNPs and GO.[27] It is worth noting that the synthesis method and process should be fully considered when fabricating antibacterial biomaterials in recent or potential bioapplications. Using the least toxic and hard-absorbed residue, an environmentally friendly and more facile synthesis strategy is usually the most popular.

In this work, we combined a facile simultaneous reduction synthesis method and a thermal evaporation-driven self-assembly technique to create RGO/AgNP hybrid films. To achieve this aim, sodium citrate, as an environmental-friendly and harmless reductant, was utilized to reduce GO and silver nitrate ($AgNO_3$) in a liquid system and then the dimension-adjustable RGO/AgNP hybrid films were fabricated by the thermal evaporation-driven self-assembly process at the liquid-air interface. Furthermore, we investigated the multi-layered structures and morphologies of the prepared RGO/AgNP hybrid films and explored their hydrophilicity. Finally, the antibacterial activity and biocompatibility of the RGO/AgNP films were demonstrated by revealing their strong abilities to kill *Escherichia coli* and promote growth of mouse osteoblast-like MC3T3-E1 cells. Based on the obtained results, we proposed a potential antibacterial mechanism for this kind of RGO/AgNP hybrid film.

2. Experimental section

2.1. Materials

Natural graphite flakes (99.8% purity), $AgNO_3$ (≥99.0% purity), and sodium citrate tribasic dehydrate (≥99.0% purity) were purchased from Sigma-Aldrich. Na_2HPO_4, NaH_2PO_4, NaCl, H_2O_2, phosphoric acid, sulphuric acid, hydrochloric acid, potassium permanganate ($KMnO_4$), ethanol, glycerol, glutaraldehyde, and diethyl ether were supplied by Beijing Chemicals Co., Ltd (Beijing, China). Dulbecco's PBS (DPBS) was pur-

chased from PAA Laboratories GmbH. A cell Counting Kit-8 (CCK-8) was bought from Dojindo Laboratories (Tokyo, Japan). All chemicals used in this work were of analytical reagent grade and directly used without additional purification. The water used was purified through a Millipore system (~18.2 MΩ cm).

2.2. Synthesis of GO

GO was synthesized by the oxidation of natural graphite flakes according to a modification of Hummers method.[28] In detail, 3 g of graphite flakes were mixed with concentrated phosphoric acid (40 mL) and sulphuric acid (360 mL) under stirring at room temperature; then potassium permanganate (18 g) was added slowly, and the mixture was incubated and stirred in a thermostatic water bath for 12 h (50 °C). When the temperature was dropped to room temperature, the mixture was poured slowly onto crushed ice (200 mL) and 10% hydrogen peroxide (10 mL). After that, the luminous yellow solution was centrifuged (4000 rpm for 0.5 h), and the supernatant was decanted away. The remaining solid material was then washed in succession with 400 mL of water, 400 mL of 30% hydrochloric acid, and 400 mL of ethanol (2×); for each wash, the supernatant decanted away. The material remaining after this multiple-wash process was coagulated with 200 mL of diethyl ether and the resulting suspension was filtered through a PTFE membrane with a 0.22 μm pore size. The obtained solid on the filter was vacuum-dried overnight at room temperature, and 6.2 g of product was obtained.

2.3. Synthesis of AgNPs

AgNPs were synthesised with sodium citrate according to a previously reported method.[29] Briefly, 11.1 mg of silver nitrate was dissolved into deionized water (65 mL). The solution in a 100 mL beaker was brought to 95 °C with magnetic stirring. Then 3.92 mL aqueous sodium citrate (1%) was added dropwise, and the reaction was allowed to run about 1 hour (when the solution reached an orange-yellow colour, which indicates the reaction was completed).

2.4. Fabrication of RGO and RGO/AgNP hybrid films

Aqueous GO (0.2 mg mL^{-1}, 60 mL) was sonicated for 1 h and heated to 95 °C in a 100 mL beaker with vigorous stirring. Then 10 mL of aqueous sodium citrate (0.5 g) was added successively into the GO solution. The reaction ran for 1 h and the final black dispersion was incubated at 80 °C to allow for formation of the RGO film. To prepare the RGO/AgNP hybrid film, a mixture of a solution of GO (0.2 mg mL^{-1}, 60 mL) and $AgNO_3$ (148 mg) was heated to 95 °C. After that, 10 mL of aqueous sodium citrate (0.75 g) was added dropwise and the reaction was continued for 1 h. Finally, the gray black dispersion was incubated at 80 °C to allow for the formation of the film.

2.5. Hydrophilicity test of RGO/AgNP film

Hydrophilicity of the fabricated RGO/AgNP hybrid films was investigated by measuring the contact angle of water droplets

on the fabricated films. The water contact angle (WCA) test was conducted with a JC2000C1 instrument. For each sample, 8–10 data points were collected and an average contact angle was calculated.

2.6. Fabrication of antibacterial material

The bacterial strain used was *Escherichia coli* (*E. coli*) ATCC 25922. Luria-Bertani (LB) broth was prepared by weighing 1 g of tryptone, 0.5 g of yeast extract, and 0.5 g of NaCl, and dissolving them in 100 mL of deionized water. This solution was autoclaved for 25 min at 116 °C prior to use. The *E. coli* were prepared as follows: a small amount of frozen *E. coli* was transferred from a −80 °C glycerol stock into 100 mL of LB media in a sterile conical flask, followed by shaking at 160 rpm and 37 °C for 14 h (WHY-2 Incubator Shaker, Changzhou Putian Instrument Manufacturing Co., Ltd). Following the 14 h incubation period, the tubes contained approximately 1×10^9 CFU (colony forming units) mL^{-1} of *E. coli*.

For the adhesion experiments, two cultures of *E. coli* were prepared as above and diluted to 1×10^3 CFU mL^{-1}. After a 14 h incubation period, 10 mL solution of each bacterial culture was transferred into a 50 mL conical tube under sterile conditions. The silicon wafers covered with and without RGO/AgNP hybrid film (1 cm × 1 cm) were first washed with 75% ethanol to kill bacteria and then put into conical tubes and incubated for 24 h at 37 °C with no shaking (DNP-9052BS-III Incubator, Shanghai CIMO Instrument Co.). Overall, 18 samples were tested in three separate runs (triplicate) of the adhesion experiment. After treating with *E. coli* bacteria solution, the morphologies characterizations of bacteria were observed with SEM. The samples were removed from the bacterial solution and delicately washed with distilled water to remove excess bacterial solution, and then dipped into stationary liquid (2.5% glutaraldehyde, solvent: 0.1 M PBS solution, pH = 7.6) for 5 h, finally dehydrated through an ethanol series (30, 40, 50, 60, 70, 80, 90, 95, and 100%, respectively) for 3 min and air-dried overnight for next characterization.

For the viability experiments, the viable cell counts of bacteria were measured by a surface spread plate method. Four sterilized samples (silicon wafers covered with no film, GO film, RGO film, and RGO/AgNP hybrid film) were immersed in 10 mL of sterilized water and inoculated with bacterial suspension (1×10^3 CFU mL^{-1}). The bacteria-inoculated solutions were incubated in a shaking incubator at 160 rpm and 37 °C. After 2 h of contact time, 100 µL of each solution was taken and cultured on melted agar (1.5%, w/v) LB solution that was allowed to solidify at room temperature before incubating overnight at 37 °C to allow viable cells to form colonies. The LB agar plates were kept at 37 °C for 24 h and the bacterial colonies were observed. Overall, 36 samples were tested in three separate runs (triplicate) of the viability experiment.

2.7. Cell culture of RGO/AgNP hybrid film

Mouse osteoblasts (MC3T3-E1 cells) were used to investigate the biocompatibility of the RGO/AgNP hybrid film. Samples transferred on silicon wafers covered with different films were washed with ethanol (70%), rinsed in Dulbecco's PBS (DPBS) and placed in a µ-slide. 300 µL of a cell suspension containing cells (1.5×10^4 cm^{-2}) were seeded into each well with incubating at 37 °C, 5% CO_2 atmosphere, and 100% humidity. The viability of cells on the samples was evaluated after being cultured for different periods. Following incubation, cells were stained with 100 µL of a vitality staining solution containing fluorescein diacetate (stock solution 0.5 mg mL^{-1} in acetone) and propidium iodide (stock solution 0.5 mg mL^{-1} in Ringer's solution). The viable and dead cells were quantified by fluorescence microscopy.

Cell proliferation was quantified using a Cell Counting Kit-8 (CCK-8) assay. Briefly, MC3T3-E1 cells were cultured in the 96-well plate with a seeding density of 5000 cells per well for 24 h. Then the culture medium was removed and replaced with fresh culture medium containing the samples (GO film, RGO film, and RGO/AgNP hybrid film) and then continuously incubated for 72 h. After that, 100 µL of fresh medium containing 10 µL of CCK-8 reagent was added to each well and incubated for an additional 4 h. Next, the plate was shaken for 300 s and absorbance was measured using single wavelength spectrophotometry at 450 nm using a microplate reader (Bio-Rad 680).

2.8. Characterization techniques

Atomic force microscopy (AFM) imaging of GO was conducted with a JPK NanoWizard 3 atomic force microscope (JPK AG, Germany) using a tapping mode. The morphology of the RGO/AgNP hybrid film was examined by scanning electron microscopy (SEM, Supra 55, Carl-Zeiss Company, Germany), which was equipped with energy dispersive X-ray spectroscopy (EDS). Transmission electron microscope (TEM) experiments were performed on a Tecnai $G^2$20 electron microscope (FEI) with an accelerating voltage of 200 kV. The final reaction suspension was directly dropped onto a copper grid, and dried at room temperature. UV-visible spectroscopy (UV-2900, Hitachi, Japan, scanning rate 400 nm min^{-1}), X-ray diffraction (XRD, Rigaku D/max-2500 VB+/PC), X-ray photoelectron spectroscopy (XPS, ThermoVG ESCALAB 250), and Raman spectroscopy (LabRAM HORIBA JY, Edison, NJ) were used to compare the structures of the GO with the RGO/AgNP hybrid film. In the antibacterial experiment, the SEM images were obtained by using a JSM-6700F scanning electron microscope (JEOL). All the fluorescence microscope images for the mouse osteoblast-like MC3T3-E1 cell test were collected with a Leica DM-IL fluorescence microscopy equipped with a Leica DFC320 camera.

2.9. Statistical analysis

All WCA and cell experiment data are expressed as the mean ± standard deviation (SD) with $n = 3$ and were analyzed using a one-way analysis of variance (ANOVA) and a Turkey-Kramer *post hoc* test using SPSS 19.0. Statistical significance was determined by analysis of variance with $P < 0.05$.

3. Results and discussion

3.1. Characterization of GO and AgNPs

GO was prepared according to the modified Hummers method involving the steps of graphite oxidation and exfoliation.[28] As shown in the AFM (Fig. 1a) and TEM (Fig. 1b) images, the single GO nanosheet with a crumpled and wrinkled structure has a height of about 1 nm (section analysis in Fig. 1a) and a size of 2–6 μm. For comparison with AgNPs in the RGO/AgNP hybrid film, pure AgNPs were synthesized and their morphologies are shown with various shapes such as a sphere, triangle, cube, and rod (Fig. 1c and d).

3.2. Fabrication and characterizations of RGO/AgNP hybrid film

Fig. 2 schematically shows the main steps for preparing the RGO/AgNP hybrid film. GO and $AgNO_3$ were mixed evenly, and then simultaneously reduced to RGO and AgNPs by the addition of sodium citrate at 95 °C (Stage 1). Meanwhile, with the temperature decreasing to 80 °C, the ash black hybrid suspension was incubated for the formation of self-assembled film at the liquid–air interface (Stage 2).

To display the reduction ability of sodium citrate, digital pictures of the prepared GO, AgNPs, RGO, and RGO/AgNP

Fig. 3   (a) Digital pictures and (b) UV spectra of GO, AgNP, RGO and RGO/AgNP hybrids; (c, d) the size distributions of pure AgNPs and AgNPs on RGO.
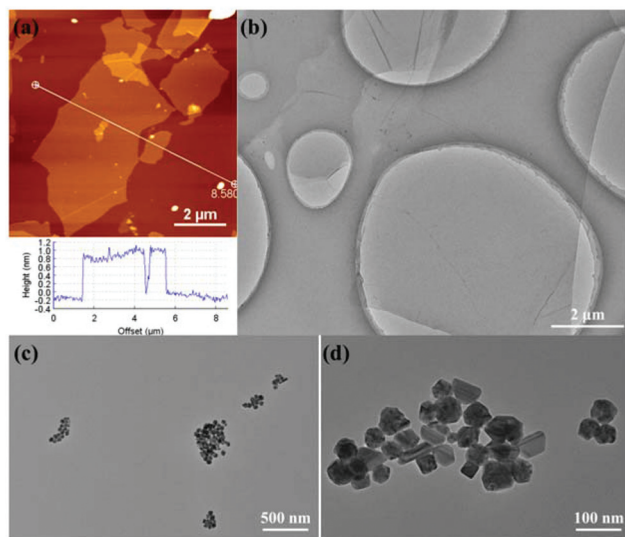

Fig. 1   Morphological and structural characterizations of GO and AgNPs: (a) AFM image and section analysis of GO, (b) TEM image of GO, (c, d) TEM images of AgNPs with different magnifications.
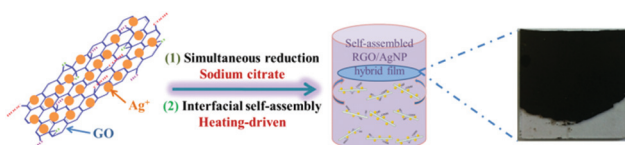

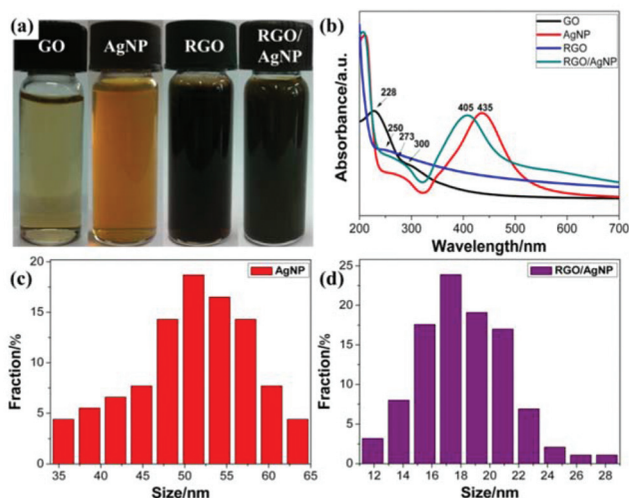Fig. 2   Schematic model for fabricating RGO/AgNP hybrid film.

were taken (Fig. 3a). The light yellow GO solution can be reduced to reddish black and ash black colour with or without $AgNO_3$. The UV-vis absorption spectrum proved to be very sensitive to the formation of silver colloids and the structure of graphene-based materials. As shown in Fig. 3b, GO exhibits a strong peak centred at 228 nm and a shoulder peak at 300 nm due to the π–π* transition of aromatic C=C bonds and n–π* transition of C=O bond, respectively.[30,31] With the reduction of sodium citrate, the absorption peak at 228 nm redshifts to 250 nm while the shoulder peak at 300 nm disappears, indicating not only the reduction of GO by sodium citrate but also the restoration of the π-conjugation network within RGO. As a "green" moderate reducing agent, sodium citrate may release free electrons and then reduce GO by them. The reaction products were small molecules such as carbon dioxide, water molecules, and so on. It should be noted that GO can't be reduced completely by this chemical reduction. In fact, the complete reduction of GO is very hard, which is different from the physical preparation of pure graphene. The physical methods can produce tiny amounts of perfect graphene with high-temperature and high-pressure equipment, while the chemical methods can obtain large amounts of RGO with different degrees of reduction by a simple process of reducing GO. Furthermore, AgNPs has a typical strong absorption peak at 435 cm, suggesting the existence of various shapes, which agrees well with the TEM results (Fig. 1c and d). However, in the UV-vis absorption spectrum of the RGO/AgNP hybrid film, both the absorption peaks of RGO and AgNPs can be observed clearly, suggesting the successful reduction of GO and $AgNO_3$ simultaneously. It should be noted that the peak at 405 nm indicates the formation of spherical AgNPs, and here the sufficient sodium citrate and high reaction temperature promote the total reduction of silver ions to AgNPs. Compared with the various shapes in pure AgNPs, the single spherical
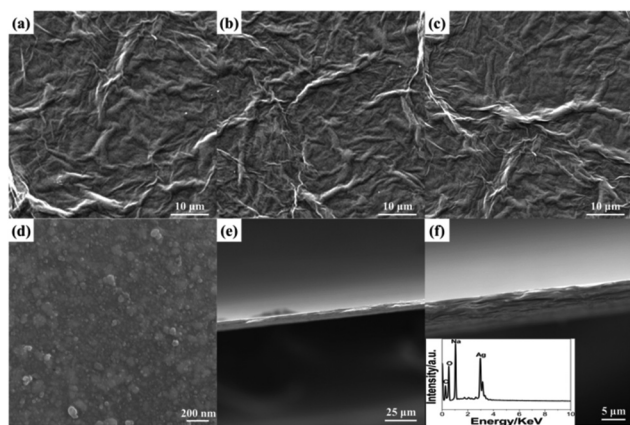
Fig. 4 SEM characterization: (a) GO film, (b) RGO film, (c, d) RGO/AgNP hybrid film with different amplifications and (e, f) cross-section analysis and EDS of the hybrid film (inset).

Fig. 5 (a–d) TEM images of RGO/AgNP suspension with different AgNP encapsulations by adjusting the mass ratio of $AgNO_3$ to GO of about 6 : 1, 8 : 1, 10 : 1, and 12 : 1, respectively.

morphology demonstrates the possible role of RGO as a good surfactant. In addition, Fig. 3c and d present the size distributions of pure AgNPs and AgNPs on RGO, in which AgNPs on RGO are much smaller than that of pure AgNPs, showing the possible role of RGO as a good surfactant for the synthesis of AgNPs.

The large-scale SEM images of GO film, RGO film, and RGO/AgNP hybrid film indicate the unique folded morphology of graphene (Fig. 4a–c), while the large-amount AgNPs are dispersed uniformly on the RGO nanosheets from the amplification of Fig. 4c (Fig. 4d). In addition, the cross-section analysis could display the multi-layered structure obviously, as shown in Fig. 4e and f. The thicker hybrid films can be obtained by delaying the evaporation time and increasing the dosages of GO and $AgNO_3$. EDS measurement was performed to investigate the chemical composition of the hybrid film. Based on the EDS analysis of the inset of Fig. 4f, it can be observed that C, O, Ag and Na were the major constituents of the sample.

As the typical synthesis feature, this self-assembly method, following a simultaneous reduction, steadily can control the dimension and thickness of the fabricated hybrid films. During the process of simultaneous reduction, the evaporation of solvent accelerates the Brownian motion and RGO nanosheets adhere to each other by the AgNPs attached on two sides as a linker. Besides, the liquid–air interface provides a suitable platform for the formation of RGO/AgNP hybrids. With the process of thermal evaporation, the complete film can be created and the accumulation results in the increased thickness of RGO/AgNP film. In addition, it should be noted that the size of the fabricated films can be effectively adjusted by using different containers and harvested with different substrates. The fabricated RGO/AgNP hybrid film can be easily transferred onto any desired substrates with different sizes.

To understand the density of AgNPs decorated on the RGO/AgNP film, the mass ratio of $AgNO_3$ to GO was adjusted and the RGO/AgNP suspensions before film formation were observed with TEM. Fig. 5 shows the typical TEM images of
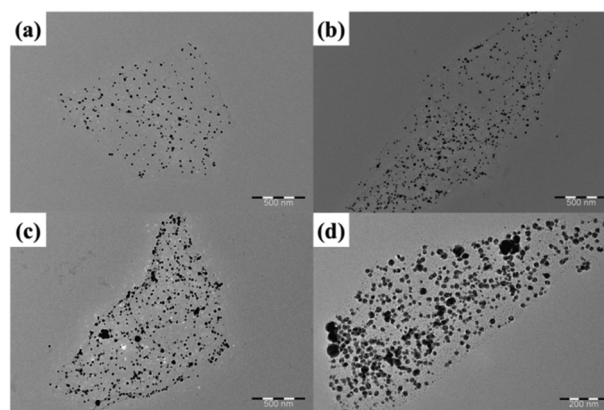
the RGO/AgNP suspensions with different decorations of AgNPs on a RGO surface. These samples were prepared by adjusting the dosage of $AgNO_3$, and the different dosages of $AgNO_3$ were 75, 100, 125, and 148 mg, which correspond to a mass ratio of $AgNO_3$ to GO of about 6 : 1, 8 : 1, 10 : 1, and 12 : 1, respectively. Based on the TEM images, the values of the top surface attached AgNPs on each sample are calculated to about 76, 123, 167, and 201 per square microns (N μm^{-2}), respectively. The diameters of the AgNPs ranged from 10 to 30 nm in all samples. In addition, the density of the AgNPs doping in the RGO/AgNP films increased with increased $AgNO_3$ concentration for the reduction reaction.

Structural characterizations of the RGO/AgNP hybrid film were performed with UV-vis spectroscopy, XRD, Raman spectroscopy, and XPS, and the corresponding results are shown in Fig. 6. The crystal structure of the RGO/AgNP hybrid film was characterized by XRD. The XRD patterns of GO and RGO were recorded for comparison (Fig. 6a). The characteristic diffraction peak (001) of GO is observed corresponding to an average interlayer spacing of ~9.35 Å, while the peak of RGO shows a dramatic shift to higher 2θ angles with spacing of ~3.71 Å, indicating that RGO is well ordered two-dimensional sheets and has smaller average interlayer spacing.[32,33] In addition, five strong diffraction peaks for the fabricated RGO/AgNP hybrid film are observed, which could be associated to the (111), (200), (220), (311) and (222) planes of the synthesized AgNPs. The diffraction peaks of the synthesized AgNPs are located in the same angles as the Joint Committee on Powder Diffraction Standards (JCPDS), strongly indicating the formation of AgNPs.[9,34]

Furthermore, Raman spectroscopy can also detect the crystalline structure of graphene-based material. Fig. 6b displays Raman spectra of the created RGO/AgNP hybrid film and its three compared samples. For all the four samples, two peaks at 1359 and 1595 cm^{-1} can be assigned to the D- and G-band, respectively. The D-band is related to the vibration of sp^3 carbon atoms of disordered graphene nanosheets, and the
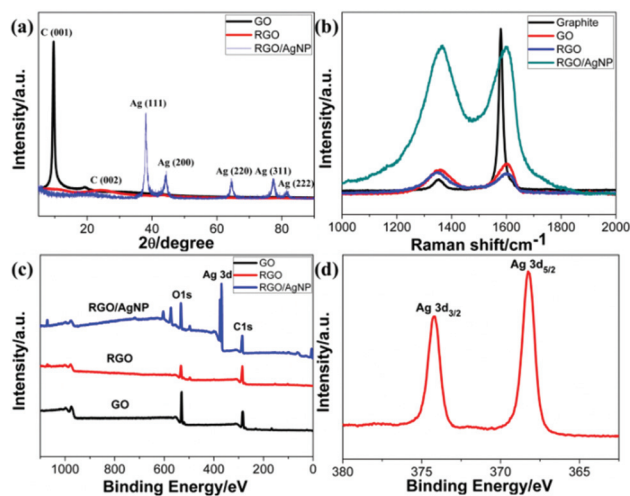
Fig. 6 Property and structure characterization of GO, RGO and RGO/AgNP hybrid film: (a) XRD patterns, (b) Raman spectra, (c, d) XPS spectra.

Fig. 7 WCA on (a) silicon wafer, (b) GO film, (c) RGO film, and (d) RGO/AgNP hybrid film.

G-band corresponds to vibration of sp^2 carbon atom domains of graphite.[35] The intensity ratios of D- and G-bands (I_D/I_G) of RGO and RGO/AgNP hybrid film increased from 0.77 to 0.97 and 1.03, respectively, indicating that most of the oxygenated groups have been removed during the reduction process. Furthermore, the D- and G-bands in RGO and RGO/AgNP hybrid film exhibit a small red shift compared with that of GO, suggesting a potential interaction between RGO and AgNPs. In addition, the intensities of D- and G-bands in the RGO/AgNP hybrid film are enhanced by ~600%. This low enhancement factor for the RGO/AgNP hybrid film indicates the presence of a chemical interaction or bonding between RGO and AgNPs.[35,36]

Fig. 6c and d shows the XPS spectra of GO, RGO, and RGO/AgNP hybrid film. For all three samples, the bands located at 284.8 and 531.0 eV are associated with the characteristic peaks of C1s and O1s, respectively.[37] Moreover, the O1s peaks of the RGO and RGO/AgNP hybrid films significantly decrease compared to that of GO, verifying the obvious deoxidation effects. In addition, Fig. 6d displays the Ag 3d spectrum, and the peaks shown in 368 (Ag $3d_{5/2}$) and 374 eV (Ag $3d_{3/2}$) provide direct evidence for the formation and decoration of AgNPs on RGO.[32,37]

3.3. Hydrophilicity test of the fabricated RGO/AgNP films

As was mentioned above, the graphene-based hybrid films have potential applications in the bio-related fields. For this purpose, hydrophilicity of the fabricated hybrid film is of great importance to the successful application.[38] In this work, hydrophilicity of the fabricated hybrid film was first investigated, and the result is shown in Fig. 7.

Three self-assembled films were transferred onto silicon wafers. Moreover, the modified silicon wafers as substrates used in all four samples were treated with boiling in a solution of concentrated sulfuric acid (70%) and hydrogen peroxide
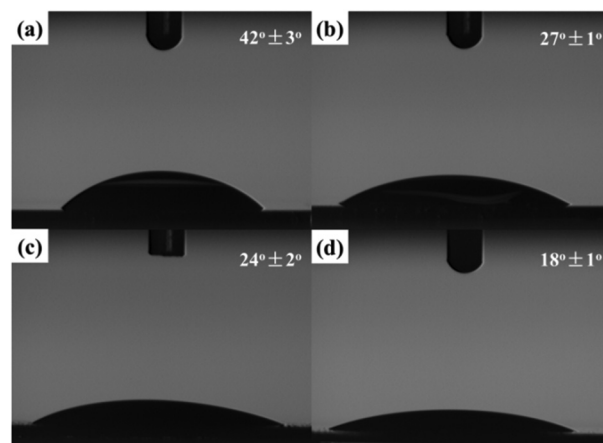
(30%) until no bubbles could be seen. In comparison with the contact angle (42 ± 3°, Fig. 7a) for the modified silicon wafer, water droplets on the self-assembled films exhibited smaller contact angles. The contact angle (24 ± 2°) of the fabricated RGO film (Fig. 7c) was a little smaller than that of the created GO film (27 ± 1°, Fig. 7b), which benefited from water-soluble reaction residues such as inorganic salts on the film during the self-assembly process. With the attachment of small nanoparticles, more specific surface area can be achieved. Therefore, the contact angle of the fabricated RGO/AgNP film with small sized AgNPs (Fig. 7d) is even decreased to about 18 ± 1°, indicating the excellent hydrophilicity of the RGO/AgNP hybrid film. Based on morphological images and the cross-section image, we suggest that the created RGO/AgNP hybrid film has a unique layer-by-layer structure. The sandwich-like and nanoporous structure of this film may be responsible for its enhanced hydrophilicity.

3.4. Antibacterial test

Recently, graphene-based nanomaterials have been found to be excellent antibacterial materials with mild cytotoxicity.[39] Previously, Kholmanov and co-workers first reported the antibacterial properties of nanostructured hybrid transparent conductive RGO/Ag-nanowire (RGO/AgNW) film.[40] Taking this fact into consideration, we further investigated antibacterial and cytotoxic properties of the prepared RGO/AgNP hybrid film. In the antibacterial test, *Escherichia coli* bacteria was chosen and studied with a typical adhesion experiment. In the adhesion experiment, two silicon wafers, covered with and without the graphene film, were immersed in separated but identical bacterial solutions and incubated overnight. The samples were then removed from the bacterial solutions and delicately washed with distilled water to remove excess bacterial solution.

The SEM image of a clean silicon wafer after this treatment (Fig. 8a) shows that a large number of *E. coli* bacteria were attached onto the silicon surface. The size of a typical bac-
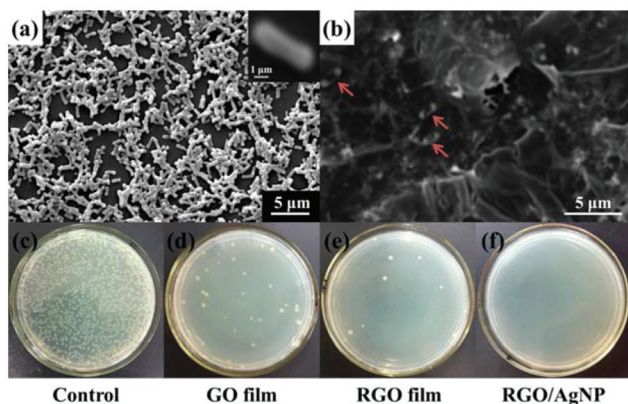
Fig. 8 Antibacterial property of RGO/AgNP hybrid film: (a, b) SEM images of (a) clean silicon wafer (a typical *E. coli* bacterium is shown in the inset) and (b) RGO/AgNP hybrid film on the surface of silicon wafer after the adhesion experiments. (c–f) Photographs of (c) clean silicon wafer, (d) GO film, (e) RGO film, and (f) RGO/AgNP hybrid film after the viability experiments. White areas correspond to bacterial colonies grown during incubation.

terium attached to the wafer is about 3 μm in length and 1.5 μm in width, as shown in the inset of Fig. 8a. It is also typically rod-shaped with smooth and intact cell walls. Comparing SEM images of bacteria on the clean silicon wafer and the RGO/AgNP hybrid film-covered silicon wafer, the wrinkled RGO sheets can be clearly seen and there are only a few bright white objects (*E. coli* bacteria) on the RGO/AgNP hybrid film-covered silicon wafer, which are marked with arrows (Fig. 8b). In addition, we can hardly find the AgNPs because of its small size and the appearance of cracks due to the long times of soaking and vibration. The presented results indicate that only a few bacteria were adhered onto the RGO/AgNP hybrid film, which reveals the antibacterial property of the synthesized film. Furthermore, the cell walls of *E. coli* on the RGO/AgNP hybrid film became wrinkled and damaged; the shape and size of these cells changed dramatically, which indicated that RGO/AgNP hybrid film exhibited strong impacts on the cell membranes of *E. coli* bacteria and destroyed bacterial cell membrane integrity.

The viability of bacteria on different substrates was further investigated. Fig. 8c–f shows the formation of bacterial colonies on the control, GO film, RGO film, and RGO/AgNP hybrid film after 24 h of cultivation. It is well known that only viable *E. coli* bacteria can form bacterial colonies. Compared with the control, GO film and RGO film revealed obvious performance to prevent the growth of bacterial colonies (Fig. 8c–e), which confirms that graphene and its derivatives can effectively inhibit the growth of *E. coli*. It should be noted that no bacterial colonies were observed on the hybrid film-covered plates, indicating the excellent performance of the RGO/AgNP hybrid film to *E. coli* bacteria (Fig. 8f). Therefore, our RGO/AgNP hybrid film shows a similar excellent antibacterial effect as the previously reported RGO/AgNW film,[40] and it is

expected that this kind of graphene film will have potential biomedical applications in the future.

A possible antibacterial mechanism of the fabricated RGO/AgNP hybrid film was proposed based on the obtained results. Previous reports indicated that AgNPs can enter into the body of bacteria directly and they have been used in many types of materials for achieving antibacterial effects.[25,27] Combining AgNPs with enzyme, the bacteria are suffocated to death. However, pure AgNPs may show less than ideal antibacterial activity, which is ascribed to the aggregation of AgNPs leading to the reduction of active specific surface area. On the other hand, graphene and graphene derivatives can induce the degradation of the inner and outer cell membranes of bacteria, and reduce their viability.[40,41] Although pure GO or RGO nanosheets cannot achieve significant performance, they play a positive role in the adhesion of bacterial to the surface of the RGO/AgNP hybrid films, which could remarkably increase the interaction between AgNPs and the bacterial surface. Therefore, based on the synergistic effects of AgNPs and RGO on antibacterial properties, the fabricated RGO/AgNP hybrid films possess excellent antibacterial performance towards *E. coli* bacteria.

The antibacterial activity of RGO/AgNP hybrid film is a comprehensive result. In fact, the antimicrobial activity of AgNPs can depend on not only AgNPs but also the remaining silver ions. The released silver ions may interact with negatively charged bacterial surfaces and induce the death of cells. In our case, the effect of silver ions on the antibacterial activity can be ignored. In addition, RGO, as the product with different reduction degrees of GO, can have a synergetic effect on antibacterial activity of the final hybrid film. The water-soluble GO nanosheets can adsorb and gather the bacteria onto the surface, which may enhance the interaction between bacteria and AgNPs on GO nanosheets.

Graphene and its derivatives may be better alternatives for fabricating novel biomaterials as they have much lesser cytotoxicity compared to other common antibacterial agents. With the combination of RGO nanosheets and AgNPs, the fabricated RGO/AgNP hybrid film, with a high specific surface area and layer-by-layer structure, showed enhanced antibacterial performance because the RGO substrates inhibited the aggregation and depletion of AgNPs. In addition, both RGO and AgNPs used for creation of the RGO/AgNP hybrid film are biocompatible, which provides enhanced biocompatibility. We suggest that this stable RGO/AgNP hybrid film will have potential applications in water purification, antibacterial materials, medical biomaterials, cell culture scaffolds, and environmental remediation.

3.5. Cell culture experiment

To evaluate biocompatibility and cytotoxicity of the created RGO/AgNP hybrid film, mouse osteoblast-like MC3T3-E1 cells were cultured on the surface of the RGO/AgNP hybrid film for the subsequent cell culture experiments.

Biocompatibility of the RGO/AgNP hybrid film was assessed by the live-dead assay *via* direct contact of cells. In this test,
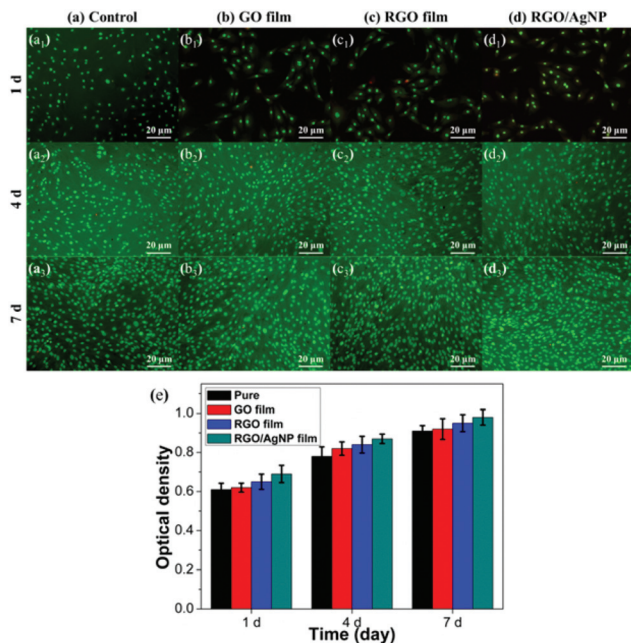
Fig. 9 (a–d) Fluorescence microscopy images of MC3T3-E1 cells (living-green; dead-red) on (a) a control, (b) GO film, (c) RGO film, and (d) RGO/AgNP hybrid film after 1, 4, and 7 days of incubation. (e) Proliferation of cells cultured on a control, GO film, RGO film, and RGO/AgNP hybrid film for 1, 4, and 7 days.

the dead cells appear in red and the living cells appear in green when observed with fluorescence microscopy. The pure MC3T3-E1 cells sample without adding film was used as a control. Fig. 9a–d shows the fluorescence microscopy images of MC3T3-E1 cells after being mixed with four kinds of substrates (a control, GO film, RGO film, RGO/AgNP hybrid film) for 1, 4, and 7 days, respectively. At the beginning, all the three samples with films have a few dead cells (red), which may be caused by the original inadaptability towards inorganic materials. However, after several days of incubation, very few dead cells can be found in any of the four samples, indicating that the MC3T3-E1 cells have excellent ability to adapt to the hybrid films. For the control sample, the number of viable cells was also found to increase with the incubation period from 1 to 7 days. It is obvious that the number of viable cells on all the four substrates increases with the incubation period distinctly, revealing the excellent biocompatibility of the MC3T3-E1 cells. Based on the above results, it can be concluded that the RGO/AgNP hybrid film exhibits very good abilities of adhesion and proliferation for cells.

To evaluate the viability of the created RGO/AgNP hybrid film, a standard CCK-8 assay was used and the result is shown in Fig. 9e. It can be observed that relative cell viability with the RGO/AgNP hybrid film is higher than that of the three other samples during the same incubation periods after the beginning, which implies that our RGO/AgNP hybrid film has no cytotoxicity to cells, but in some way has a significant promotion on cell growth.

Previous studies indicate that both graphene and AgNPs have biological applications.[42–45] For instance, large-scale two-dimensional graphene film has been fabricated and utilized for the cell growth,[43–45] and AgNPs have been used in human cells.[46] However, the types and proportions of the functional groups on the surfaces of graphene derivatives (GO and RGO) can influence the biological properties significantly. In addition, nanomaterials such as AgNPs can process unique properties with synthetic control of size, uniformity, morphology and structure. Therefore, the performances of cytotoxicity and cell growth were the reflection of complex interactions effects. The cell-promoted performance of our RGO/AgNP hybrid film may be ascribed to the small sized AgNPs and RGO. We suggest that AgNPs serve as good adhesion sites for cells from chemical bonding and thus RGO nanosheets provide an excellent two-dimensional scaffold for cell adhesion and growth. After long-term cell culture experiments (about one week), the fabricated scaffold did not show any decomposition in this biological system. In addition, we tested the stability of this hybrid film in different solutions, like water and buffers, and found that this kind of RGO/AgNP hybrid film is very stable. The strong stability of this film is ascribed to its multi-layered structure, in which AgNPs and RGO nanosheets connect each other. Based on the above cell culture results, we suggest that the created RGO/AgNP hybrid film has favourable biocompatibility and it can be used as a new scaffold for cell growth and as a potential novel nano-carrier for drug delivery.[47]

4.   Conclusions

We present a facile strategy for the preparation of dimension-adjustable multi-layered RGO/AgNP hybrid films by combining a simultaneous reduction and a thermal evaporation-driven self-assembly process. Thicker hybrid films can be obtained by delaying the evaporation time and increasing the dosages of GO and AgNO$_3$. Moreover, we can transfer it onto a selected substrate for further applications without any post process. The prepared RGO/AgNP hybrid films exhibit outstanding hydrophilicity. Compared to previous methods of fabricating graphene-based hybrid films, our strategy has several advantages, such as environmental friendliness, no additives, time saving, high efficiency, and cost-effectiveness. Finally, the created RGO/AgNP hybrid film can be transferred directly onto silicon wafers for antibacterial and cell culture applications without any further complex post process. This facile strategy shown in this work opens up a new way to prepare diverse graphene-based hybrid films and extends the potential applications in biomedicine, biomaterials, and drug delivery.

Acknowledgements

Notes and references

1 B. D. Bax, P. F. Chan, D. S. Eggleston, A. Fosberry, D. R. Gentry, F. Gorrec, I. Giordano, M. M. Hann, A. Hennessy, M. Hibbs, J. Huang, E. Jones, J. Jones, K. K. Brown, C. J. Lewis, E. W. May, M. R. Saunders, O. Singh, C. E. Spitzfaden, C. Shen, A. Shillings, A. J. Theobald, A. Wohlkonig, N. D. Pearson and M. N. Gwynn, *Nature*, 2010, **466**, 935.
2 R. Wise, *J. Antimicrob. Chemother.*, 2011, **66**, 1939.
3 I. Francolini, L. D'Ilario, E. Guaglianone, G. Donelli, A. Martinelli and A. Piozzi, *Acta Biomater.*, 2010, **6**, 3482.
4 O. Wiarachai, N. Thongchul, S. Kiatkamjornwong and V. P. Hoven, *Colloids Surf., B*, 2012, **92**, 121.
5 S. J. Yuan, S. O. Pehkonen, Y. P. Ting, K. G. Neoh and E. T. Kang, *Langmuir*, 2010, **26**, 6728.
6 A. V. Fuchs, S. Ritz, S. Pütz, V. Mailänder, K. Landfester and U. Ziener, *Biomater. Sci.*, 2013, **1**, 470.
7 V. Etacheri, G. Michlits, M. K. Seery, S. J. Hinder and S. C. Pillai, *ACS Appl. Mater. Interfaces*, 2013, **5**, 1663.
8 T. Kavitha, A. I. Gopalan, K. P. Lee and S. Y. Park, *Carbon*, 2012, **50**, 2994.
9 L. Liu, J. Liu, Y. Wang, X. Yan and D. D. Sun, *New J. Chem.*, 2011, **35**, 1418.
10 C. Krishnaraj, E. G. Jagan, S. Rajasekar, P. Selvakumar, P. T. Kalaichelvan and N. Mohan, *Colloids Surf., B*, 2010, **76**, 50.
11 B. Jia, Y. Mei, L. Cheng, J. Zhou and L. Zhang, *ACS Appl. Mater. Interfaces*, 2012, **4**, 2897.
12 R. J. B. Pinto, P. A. A. P. Marques, C. P. Neto, T. Trindade, S. Daina and P. Sadocco, *Acta Biomater.*, 2009, **5**, 2279.
13 X. Fei, M. Jia, X. Du, Y. Yang, R. Zhang, Z. Shao, X. Zhao and X. Chen, *Biomacromolecules*, 2013, **14**, 4483.
14 V. Georgakilas, M. Otyepka, A. B. Bourlinos, V. Chandra, N. Kim, K. C. Kemp, P. Hobza, R. Zboril and K. S. Kim, *Chem. Rev.*, 2012, **112**, 6156.
15 S. Guo and S. Dong, *Chem. Soc. Rev.*, 2011, **40**, 2644.
16 X. Huang, X. Qi, F. Boey and H. Zhang, *Chem. Soc. Rev.*, 2012, **41**, 666.
17 X. Zhao, P. Zhang, Y. Chen, Z. Su and G. Wei, *Nanoscale*, 2015, **7**, 5080.
18 H. W. Tien, Y. L. Huang, S. Y. Yang, J. Y. Wang and C. C. M. Ma, *Carbon*, 2011, **49**, 1550.
19 D. Lee, H. Lee, Y. Ahn, Y. Jeong, D. Y. Lee and Y. Lee, *Nanoscale*, 2013, **5**, 7750.
20 P. Zhang, Y. Huang, X. Lu, S. Zhang, J. Li, G. Wei and Z. Su, *Langmuir*, 2014, **30**, 8980.
21 J. Wang, X. Zhao, J. Li, X. Kuang, Y. Fan, G. Wei and Z. Su, *ACS Macro Lett.*, 2014, **3**, 529.
22 J. Z. Wang, C. Zhong, S. L. Chou and H. K. Liu, *Electrochem. Commun.*, 2010, **12**, 1467.
23 I. Ocsoy, M. L. Paret, M. A. Ocsoy, S. Kunwar, T. Chen, M. You and W. Tan, *ACS Nano*, 2013, **7**, 8972.
24 S. Dutta, C. Ray, S. Sarkar, M. Pradhan, Y. Negishi and T. Pal, *ACS Appl. Mater. Interfaces*, 2013, **5**, 8724.
25 W. Hu, C. Peng, W. Luo, M. Lv, X. Li, D. Li, Q. Huang and C. Fan, *ACS Nano*, 2010, **4**, 4317.
26 M. Moritz and M. Geszke-Moritz, *Chem. Eng. J.*, 2013, **228**, 596.
27 J. Ma, J. Zhang, Z. Xiong, Y. Yong and X. S. Zhao, *J. Mater. Chem.*, 2011, **21**, 3350.
28 D. C. Marcano, D. V. Kosynkin, J. M. Berlin, A. Sinitskii, Z. Sun, A. Slesarev, L. B. Alemany, W. Lu and J. M. Tour, *ACS Nano*, 2010, **4**, 4806.
29 D. Steinigeweg and S. Schlücker, *Chem. Commun.*, 2012, **48**, 8682.
30 D. Li, M. B. Müller, S. Gilje, R. B. Kaner and G. G. Wallace, *Nat. Nanotechnol.*, 2008, **3**, 101.
31 J. Tang, Q. Chen, L. Xu, S. Zhang, L. Feng, L. Cheng, H. Xu, Z. Liu and R. Peng, *ACS Appl. Mater. Interfaces*, 2013, **5**, 3867.
32 Y. Zhou, J. Yang, X. Cheng, N. Zhao, H. Sun and D. Li, *RSC Adv.*, 2013, **3**, 3391.
33 X. Zhao, Y. Li, J. Wang, Z. Ouyang, J. Li, G. Wei and Z. Su, *ACS Appl. Mater. Interfaces*, 2014, **6**, 4254.
34 W. P. Xu, L. C. Zhang, J. P. Li, Y. Lu, H. H. Li, Y. N. Ma, W. D. Wang and S. H. Yu, *J. Mater. Chem.*, 2011, **21**, 4593.
35 Z. Xu, H. Gao and G. Hu, *Carbon*, 2011, **49**, 4731.
36 K. Jasuja and V. Berry, *ACS Nano*, 2009, **3**, 2358.
37 Y. Zhang, S. Liu, L. Wang, X. Qin, J. Tian, W. Lu, G. Chang and X. Sun, *RSC Adv.*, 2012, **2**, 538.
38 L. Yan, Y. B. Zheng, F. Zhao, S. Li, X. Gao, B. Xu, P. S. Weiss and Y. Zhao, *Chem. Soc. Rev.*, 2012, **41**, 97.
39 T. S. Sreeprasad, M. S. Maliyekkal, K. Deepti, K. Chaudhari, P. L. Xavier and T. Pradeep, *ACS Appl. Mater. Interfaces*, 2011, **3**, 2643.
40 I. N. Kholmanov, M. D. Stoller, J. Edgeworth, W. H. Lee, H. Li, J. Lee, C. Barnhart, J. R. Potts, R. Piner, D. Akinwande, J. E. Barrick and R. S. Ruoff, *ACS Nano*, 2012, **6**, 5157.
41 Y. Tu, M. Lv, P. Xiu, T. Huynh, M. Zhang, M. Castelli, Z. Liu, Q. Huang, C. Fan, H. Fang and R. Zhou, *Nat. Nanotechnol.*, 2013, **8**, 594.
42 G. Y. Chen, D. W. P. Pang, S. M. Hwang, H. Y. Tuan and Y. C. Hu, *Biomaterials*, 2012, **33**, 418.
43 H. Wang, D. Sun, N. Zhao, X. Yang, Y. Shi, J. Li, Z. Su and G. Wei, *J. Mater. Chem. B*, 2014, **2**, 1362.
44 J. Wang, H. Wang, Y. Wang, J. Li, Z. Su and G. Wei, *J. Mater. Chem. B*, 2014, **2**, 7360.
45 H. Chen, M. B. Müller, K. J. Gilmore, G. G. Wallace and D. Li, *Adv. Mater.*, 2008, **20**, 3557.
46 P. V. AshaRani, G. L. K. Mun, M. P. Hande and S. Valiyaveettil, *ACS Nano*, 2009, **3**, 279.
47 S. Kim, S. H. Ku, S. Y. Lim, J. H. Kim and C. B. Park, *Adv. Mater.*, 2011, **23**, 2009.